The Formation of Performance Enhancing Pseudo-Composites in the Highly Active $La_{1-x}Ca_xFe_{0.8}Ni_{0.2}O_3$ System for IT-SOFC Application

*Nagore Ortiz-Vitoriano, Idoia Ruiz de Larramendi, Stuart N. Cook, Mónica Burriel, Ainara Aguadero, John A. Kilner, and Teófilo Rojo**

The $La_{1-x}CaxFe_{0.8}Ni_{0.2}O_{3-\delta}$ ($0 \leq x \leq 0.9$) system is investigated for potential application as a cathode material for intermediate temperature solid oxide fuel cells (IT-SOFCs). A broad range of experimental techniques have been utilized in order to elucidate the characteristics of the entire compositional range. Low A-site Ca content compositions ($x \leq 0.4$) feature a single perovskite solid solution. Compositions with 40% Ca content ($x = 0.4$) exhibit the highest electrical and ionic conductivities of these single phase materials (250 and 1.9×10^{-3} S cm^{-1} at 800 °C, respectively), a level competitive with state-of-the-art (La,Sr)(Fe,Co)O_3. Between 40 and 50% Ca content ($0.4 > x > 0.5$) a solubility limit is reached and a secondary, brownmillerite-type phase appears for all higher Ca content compositions ($0.5 \leq x \leq 0.9$). While typically seen as detrimental to electrochemical performance in cathode materials, this phase brings with it ionic conductivity at operational temperatures. This gives rise to the effective formation of pseudo-composite materials which feature significantly enhanced performance characteristics, while also providing the closest match in thermal expansion behavior to typical electrolyte materials. This all comes with the advantage of being produced through a simple, single-step, low-cost production route without the issues associated with typical composite materials. The highest performing pseudo-composite material ($x = 0.5$) exhibits electronic conductivity of 300–350 S cm^{-1} in the 600–800 °C temperature range while the best polarisation resistance (R_p) values of approximately 0.2 Ω cm^2 are found in the $0.5 \leq x \leq 0.7$ range.

1. Introduction

A solid oxide fuel cell (SOFC) directly converts chemical to electrical energy and has been shown to be a good candidate for distributed power applications. In order to limit cathodic overpotential in a typical SOFC, operation temperatures remain in the 800–1000 °C range. These high temperatures are, however, accompanied by associated issues such as cell degradation and the consequent maintenance costs which limit their commercial use.[1] An effective approach in overcoming these issues is the reduction of operating temperature to the 600–800 °C, so-called intermediate temperature (IT), range. This provides a number of benefits, including greater versatility in cell material choice, prolonged lifetime and reduced manufacturing costs.[2,3]

Desirable characteristics for IT-SOFC cathodes include mixed ionic and electronic conductivity (MIEC) and a good match in thermal expansion coefficient (TEC) with the electrolyte. Cathode material development has primarily focused on perovskites with the general formula ABO_3 (A = La, B = Fe, Co, Ni) doped with Sr or Ca, with the highest performance coming from the $La_{1-x}Sr_xFe_{1-y}Co_yO_3$ system.[4] Unfortunately, these cathodes have shortcomings associated with the use of Co, which is very expensive and is responsible for the high TEC values usually found in these materials.[5]

A-site doped lanthanum orthoferrites ($La_{1-x}A_xFeO_3$) have been reported to exhibit high catalytic activity and MIEC at reduced temperatures (σ_e total > 100 S cm^{-1} at 600–800 °C).[6] With an ionic radius of 1.36 Å, La provides an excellent A-site cation for an oxide ion conducting perovskite. The substitution of the trivalent La on the A-site with divalent Sr (1.44 Å) or Ca (1.34 Å) introduces MIEC to the perovskite through the formation of oxygen vacancies and/or oxidation of Fe to achieve overall charge neutrality. The use of Ca as an A-site dopant has advantages over Sr such as a lower raw material cost and closer ionic radius to La^{3+}; Ca- doped materials, however, typically present lower levels of ionic conductivity.[7] Sr

Dr. N. Ortiz-Vitoriano, Dr. I. R. de Larramendi, Prof. T. Rojo
Departamento de Química Inorgánica
Facultad de Ciencia y Tecnología
Universidad del País Vasco UPV/EHU
Apdo. 644, 48080 Bilbao, Spain
E-mail: teo.rojo@ehu.es
Dr. S. N. Cook, Dr. M. Burriel, Dr. A. Aguadero, Prof. J. A. Kilner
Department of Materials
Imperial College London
Prince Consort Rd, London SW7 2BP, UK
Prof. J. A. Kilner, Prof. T. Rojo
CIC energiGUNE
Parque Tecnológico de Álava
Albert Einstein 46 - ED. E7, 01510 Miñano, Álava, Spain

DOI: 10.1002/adfm.201300481

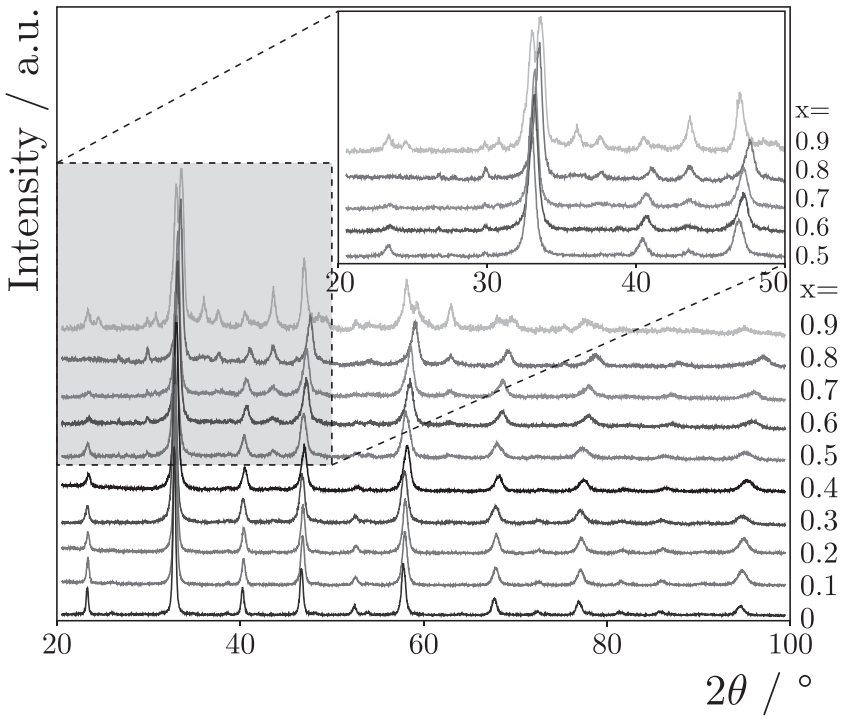

Figure 1. X-ray diffraction patterns of $La_{1-x}Ca_xFe_{0.8}Ni_{0.2}O_{3-\delta}$ ($0 \le x \le 0.9$) samples. Inset: detailed portion of the patterns showing the peaks corresponding to the new phase.

is also known to diffuse through the electrolyte at the high temperatures involved in manufacture, leading to severe cell performance degradation.[8,9] Transition metal ion doping on the Fe B-site has resulted in interesting electrical properties, an example being the $LaNi_{0.2}Fe_{0.8}O_3$ phase ($\sigma = 135$ S cm^{-1} at 800 °C), although Fe-rich phases are more thermodynamically stable.[10,11]

While a large number of studies in mixed conducting perovskites report the presence of secondary phases, they are often left unidentified[6,12,13] and are typically considered undesirable and associated with low conductivity values and poor performance.[14] Conversely, the majority of SOFC cathodes are actually composite in nature, as the inherent requirements are so wide-ranging that no single material is capable of fulfilling every aspect.[15] Composite cathodes provide enhanced catalytic activity, often through the addition of a fast ionic conductor to improve oxygen ion transport to active reaction sites[16] as in the $La_{0.6}Ca_{0.4}Fe_{0.8}Ni_{0.2}O_{3-\delta}$/samarium doped ceria (SDC) symmetrical cells reported in a previous work.[17] Investigated composite cathodes include $Sm_{0.5}Sr_{0.5}CoO_3$ (SSC)-$Ce_{0.8}Sm_{0.2}O_{1.9}$ (SDC), $La_{0.6}Sr_{0.4}Co_{0.2}Fe_{0.8}O_3$ (LSCF)-SDC, LSCF-$Ce_{0.8}Gd_{0.2}O_2$ (CGO) and $Ba_{0.5}Sr_{0.5}Co_{0.2}Fe_{0.8}O_3$ (BSCF)-SDC, all of which exhibit low polarisation resistance at 600 °C.[18,19] The electrochemical performance of these cathodes is generally governed by triple phase boundary (TPB) kinetics, mass transport and ohmic drop.[20] The primary disadvantages of using composite materials arise from the need for two independent materials; this increases both production complexity and the possibility of undesirable phases forming through inter-reaction of the component phases.

In this work, the $La_{1-x}Ca_xFe_{0.8}Ni_{0.2}O_{3-\delta}$ (LCFN) system is investigated, revealing the appearance of a secondary, ion conducting, brownmillerite-structured phase which results in a high performance, pseudo-composite cathode. This presents an advantage over typical cathode composites as it is produced by means of a single, low temperature processing route. The shorthand notation of LCFN*x* will be used throughout, where *x* represents calcium content in the nominal compositional formula $La_{1-x}Ca_xFe_{0.8}Ni_{0.2}O_{3-\delta}$.

2. Results and Discussion

2.1. Crystal Structure

X-ray diffraction (XRD) patterns obtained at room temperature of $La_{1-x}Ca_xFe_{0.8}Ni_{0.2}O_{3-\delta}$ ($0 \le x \le 0.9$) solid solutions are shown in **Figure 1**. The phases were initially indexed to an orthorhombic perovskite structure with the space group P*nma* (no.62); similar to those of $LaFeO_3$[21] and $Ln_{0.6}Ca_{0.4}FeO_3$.[22] In compositions with Ca content (*x*) greater than 0.5 secondary phases were identified, discussed shortly.

Changes in the crystal structure of the single phase, perovskite materials ($x \le 0.4$) determined from Rietveld refinement of XRD patterns are plotted against Ca content in **Figure 2**a,b and their values (Supporting Information) are in good agreement with literature.[23] The *b* cell parameter increases up to a peak at $x = 0.3$, with a subsequent decrease. The *a* and *c* parameters show the inverse trend with a decrease until $x = 0.3$ and then an increase. A systematic decrease in volume with increasing doping level is observed; when Ca content increases from $x = 0$ to $x = 0.4$, the unit cell volume decreases from 240.538 to 239.209 Å^3. This is due to the decrease in A-site cation radius with the substitution of La^{3+} (1.36 Å) for the smaller Ca^{2+} (1.34 Å),[24] as well as a change in the Fe-site mean ionic radius; a result of charge compensation of the divalent Ca substitution on the trivalent La site. The oxidation of Fe^{3+} results in a change in mean site ionic radius ($<r_{Fe}>$) from the larger Fe^{3+} (0.645 Å) to the smaller Fe^{4+} (0.585 Å).[25] Taguchi et al. and Ahmed et al. observed a similar trend in the $La_{1-x}Ca_xFeO_3$ system and Bellakki et al. in the $La_{1-x}Cd_xFeO_3$ ($0 \le x \le 0.3$) system.[12,26,27]

Change in Fe-site mean ionic radius also affects the bond lengths and bond angles of the FeO_6 octahedra, which are reflective of the degree of orthorhombic distortion and octahedra tilting, respectively (Figure 2b). A decrease in the average Fe-O bond length can be attributed to the previously mentioned Fe^{3+} to Fe^{4+} size reduction. Similarly, the Fe-O_1-Fe bond angle increases and Fe-O_2-Fe decreases, indicating distortion as more Fe^{4+} is introduced, as a consequence of the Jahn-Teller effect.

Attempts to introduce a greater level of Ca doping ($x \ge 0.5$) results in the segregation of a secondary $Ca_2Fe_2O_5$–type (brownmillerite, space group: *Pnma*) phase. Peaks from this phase

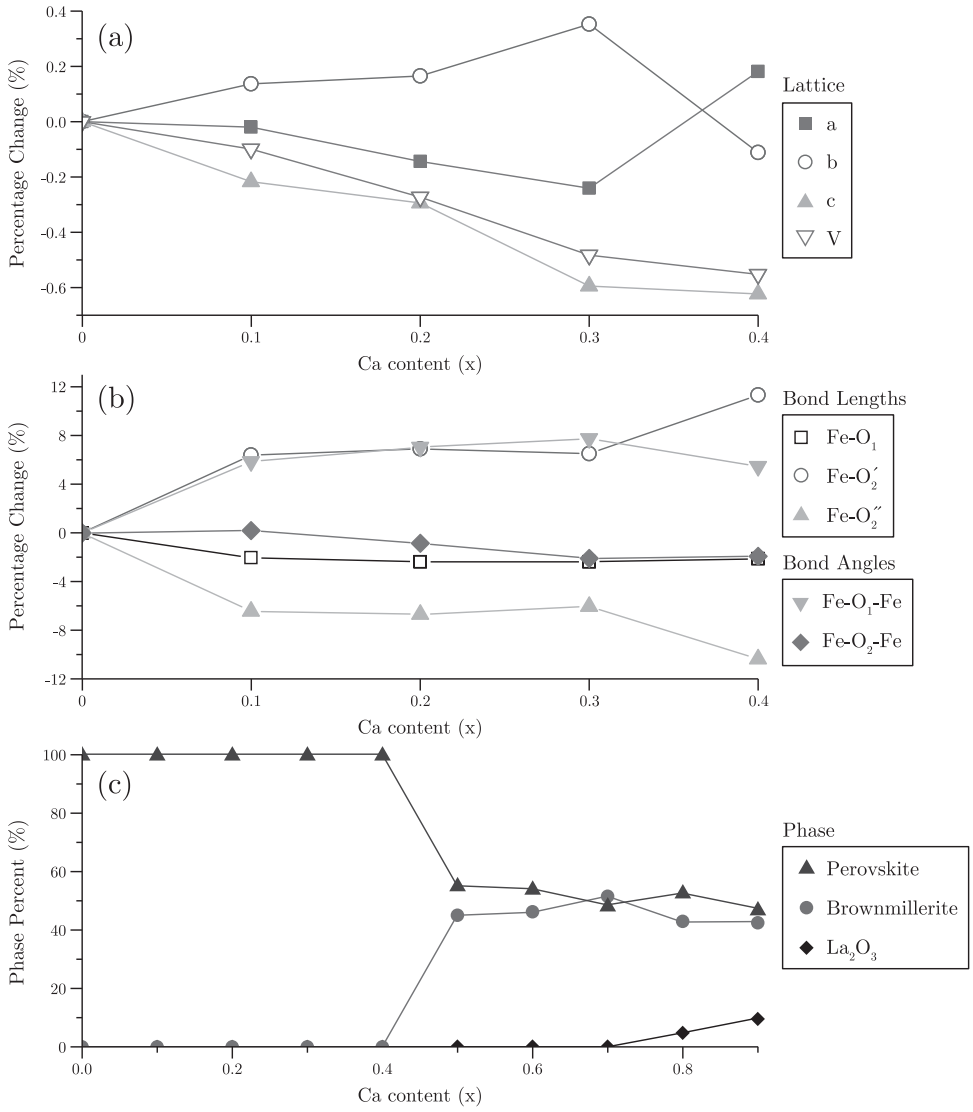

Figure 2. Features of the perovskite phase determined through XRD pattern refinement for $La_{1-x}Ca_xFe_{0.8}Ni_{0.2}O_{3-\delta}$ samples against Ca content x: a) lattice parameters, b) Fe-O bond characteristics for $0 \leq x \leq 0.4$ and c) phase proportions for $0 \leq x \leq 0.9$.

are highlighted in the inset in Figure 1. The appearance of this brownmillerite phase is also reported by other authors[28,29] and the lattice parameters of $a = 5.24$ Å, $b = 15.10$ Å and $c = 5.52$ Å (in LCFN0.7 sample) agree well with those in literature.[30,31] Nominal compositions with a high level of Ca content ($x \geq 0.8$) feature an additional lanthanum oxide (La_2O_3) phase. The phase fractions for all nominal compositions are shown against calcium content in Figure 2c. Additional results from these refined XRD patterns including plotted and tabulated data can be found in the Supporting Information.

While it is important to determine the crystal structure of the materials at room temperature, the high operating temperatures (>600 °C) of SOFC systems make it essential to develop an understanding of the behavior and stability of these materials at high temperature. In order to ascertain this, XRD measurements were performed as a function of temperature from 30 to 1050 °C.

Three-dimensional plots and two-dimensional heat maps of the recorded diffraction patterns for the compositions with $x = 0.1$, 0.5 and 0.9 are shown in **Figure 3**. LCFN0.1 shows an increase in crystallinity with increasing temperature but no formation of any additional phases and the perovskite structure remains unchanged within the temperature range investigated. However, the appearance of two new peaks at 36.8° and 42.8° (2θ) is observed for the LCFN0.5 and LCFN0.9 compositions at roughly 850 °C. The peak observed at 42.8° could be due to a structural phase transition from *Pnma* to *Icmm* in the brownmillerite phase.[32] The peak observed at 36.8° was identified as Fe_2O_3 which was also observed by Berastegui et al. in the $Ca_2Fe_2O_5$ system.[32] As can be seen in Figure 3b, an increase in crystallinity with temperature results in an intense diffraction peak at 32.6°, suggesting an increase in crystallite size. However, the most intense diffraction peak for the LCFN0.9 composition is a mixture of perovskite, brownmillerite and La_2O_3.

ADVANCED FUNCTIONAL MATERIALS
www.afm-journal.de

www.MaterialsViews.com

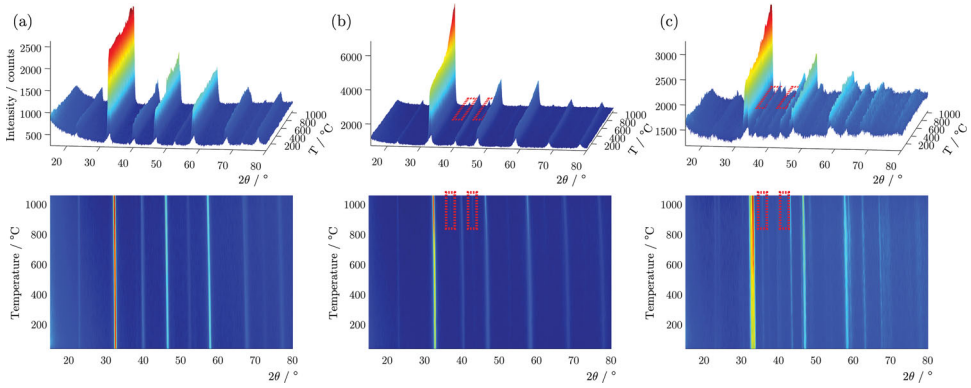

Figure 3. X-Ray thermodiffractograms of a) $La_{0.9}Ca_{0.1}Fe_{0.8}Ni_{0.2}O_{3-\delta}$, b) $La_{0.5}Ca_{0.5}Fe_{0.8}Ni_{0.2}O_{3-\delta}$ and c) $La_{0.1}Ca_{0.9}Fe_{0.8}Ni_{0.2}O_{3-\delta}$ from room temperature to 1050 °C. High temperature phase segregation highlighted in red.

Furthermore, the appearance of these new phases becomes more significant for the composition with 90% Ca. The results of the Rietveld refinement for the LCFN0.9 sample at 1050 °C are given in the Supporting Information. The analysis of this data reveals perovskite, brownmillerite, lanthanum oxide and iron oxide proportions of 46.6, 38.9, 10.5 and 3.8%, respectively. The appearance of the lanthanum oxide and iron oxide phases at high temperatures in materials with Ca content x between 0.5 and 0.9 effectively limits their use as cathodes to below 850 °C, making them suitable for use in IT-SOFCs, while those with x lower than 0.5 are not limited in the temperature range measured.

2.2. Microstructure and Thermal Expansion Properties

The electrochemical properties of the samples are influenced not only by the structural features but also by particle size. Phases featuring smaller particle size exhibit behavior more suited to cathode application making the investigation of sample morphology important,[33] as reported in $La_{0.8}Ca_{0.2}Fe_{0.8}Ni_{0.2}O_{3-\delta}$ material.[34] Scanning electron microscopy (SEM) images of the LCFN samples are shown in **Figure 4**. A range of particle size distributions and levels of agglomeration are observed. The level of porosity increases with Ca content up to $x = 0.4$ and then the particles tend to agglomerate giving rise to an overall coarsening of the morphology with particle sizes larger than 100 nm. This increase in particle size with alkaline earth content was also observed by Vidal et al. for the $AFeO_{3-\delta}$ (A = $Ln_{1-x}M_x$; Ln = La, Nd and/or Pr; M = Sr and/or Ca) system.[25] This is a result of the decrease in melting point with Ca content in a similar manner to that observed between $LaFeO_3$ and $CaFeO_3$.[35,36] Kharton et al. report that this gives rise to liquid-phase assisted sintering and enhanced grain growth.[37]

The thermal expansion coefficients (TECs) of all compositions were measured by dilatometry. The thermal expansion behavior is strongly dependent on calcium dopant content with the TEC seen to decrease in an approximately linear fashion with increasing Ca content, from 15.8×10^{-6} K^{-1} to 11.1×10^{-6} K^{-1} at $x = 0$ and 0.9, respectively. This trend is in good agreement with the findings of Petric and Ullman for cobalt ferrites.[38,39] This behavior can be attributed to several effects;

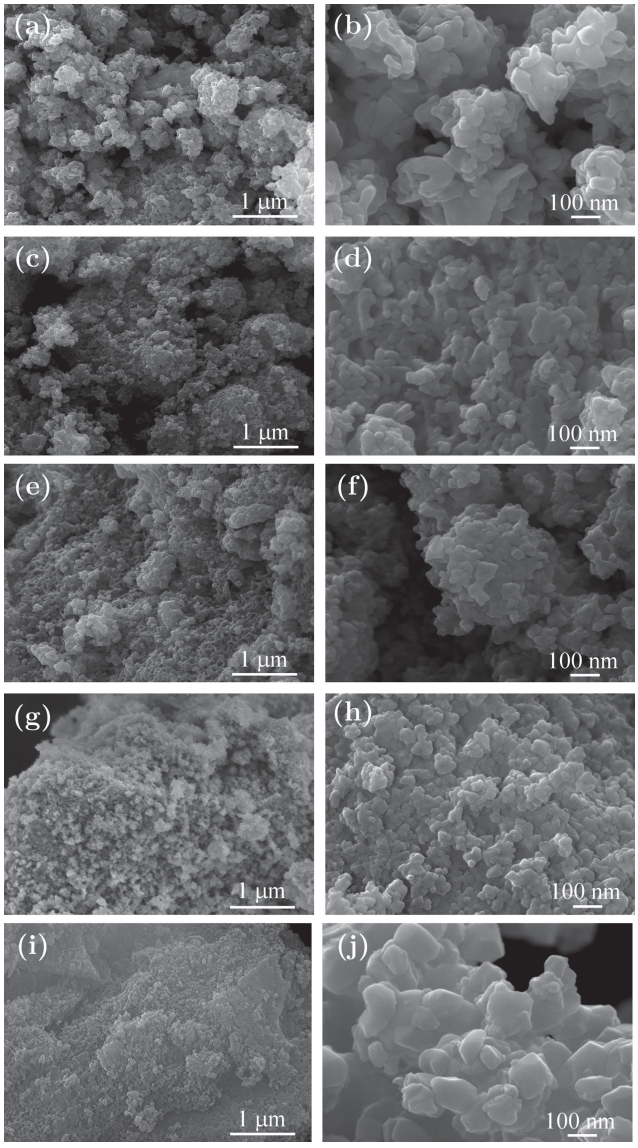

Figure 4. SEM images obtained at 20 000 and 100 000 times magnification for a,b) $LaFe_{0.8}Ni_{0.2}O_{3-\delta}$, c,d) $La_{0.8}Ca_{0.2}Fe_{0.8}Ni_{0.2}O_{3-\delta}$, e,f) $La_{0.6}Ca_{0.4}Fe_{0.8}Ni_{0.2}O_{3-\delta}$, g,h) $La_{0.4}Ca_{0.6}Fe_{0.8}Ni_{0.2}O_{3-\delta}$, and i,j) $La_{0.2}Ca_{0.8}Fe_{0.8}Ni_{0.2}O_{3-\delta}$.

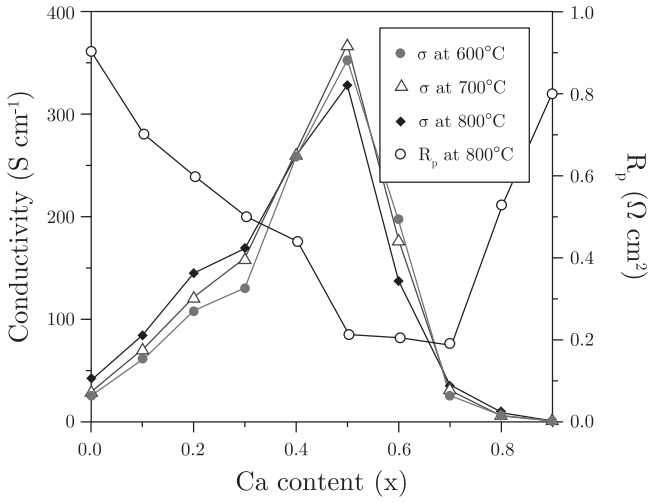

Figure 5. Effect of the Ca^{2+} content on the electrical conductivity (σ) at a range of temperatures and R_p at 800 °C.

the different ionic radii of La^{3+} (1.36 Å) and Ca^{2+} (1.34 Å),[24] the partial oxidation of Fe^{3+} to Fe^{4+} which induces an overall shortening of the bond lengths, and to the appearance of the brownmillerite phase which has a lower TEC in the temperature range, 700–1000 °C (11.3×10^{-6} K^{-1} in $Ca_2Fe_2O_5$[40]). The thermal expansion behavior and its dependence on Ca content are plotted in the Supporting Information (Figure S2, Supporting Information). LCFN samples with Ca content x between 0.5 and 0.6 are the most thermomechanically compatible materials with SDC electrolytes (12.7×10^{-6} K^{-1}).[41]

2.3. Electrochemical Performance and Oxygen Vacancy Content

The electrical conductivity (σ) of the $La_{1-x}Ca_xFe_{0.8}Ni_{0.2}O_{3-\delta}$ compositions in air is shown in **Figure 5**. Total electrical conductivity includes both electronic and ionic contributions due to the presence of holes and oxygen vacancies, respectively. In this type of lanthanum orthoferrite perovskite oxide the ionic conductivity can be considered negligible in comparison with the overall conductivity. This is proven to be true later in this work by way of isotopic tracer diffusion measurements with ionic contributions to the conductivity at least 3 orders of magnitude lower than total conductivity. Reported conductivity can therefore be considered electronic in nature.[42] The conductivity is seen to reach a maximum with 50% Ca dopant on the La site. The almost linear rise with increasing Ca up to this point is consistent with studies on acceptor-doped $LaFeO_3$.[43] Conversely, at higher Ca levels (>50%) the conductivity is seen to rapidly decline.

The increase in conductivity with temperature for samples with low Ca content ($0 \leq x \leq 0.3$) is consistent with the thermally activated, p-type, small polaron hopping mechanism previously reported in A-site-doped lanthanum orthoferrite perovskites.[44–46] This trend is not maintained at greater Ca content, however, which may be related to the appearance of the brownmillerite ($Ca_2Fe_2O_5$) secondary phase reported previously by XRD studies. At low temperatures hole-type electronic conduction is present due to oxygen interstitials in the $Ca_2Fe_2O_5$ structure, while at temperatures greater than 677 °C a phase transition (*Pnma–Icmm*) is reported to take place resulting in a lower level of oxygen and thus lower electrical conduction.[47,48] Materials of this sort have attracted a great deal of attention due to their ability to accommodate a large number of oxygen vacancies in the lattice, resulting in fast oxygen ionic conductivity.[49,50]

This study implies that the partial substitution of Ca^{2+} in the A-site together with Ni^{2+} in the B-site of the $LaFeO_3$ perovskite has an enhancing effect on electrical conductivity up to 60% Ca when compared with $La_{1-x}Ca_xFeO_3$.[51] The conductivity is over 100 S cm^{-1} at temperatures greater than 600 °C for materials with Ca content between 0.2 and 0.6, satisfying the general requirement for electrode materials in IT-SOFCs.[52]

The thermal evolution of the oxygen content of the samples was evaluated by thermal analysis. **Figure 6**a shows the mass loss observed for LCFN0.6 during the second heating-cooling cycle. The sample displays a regular reduction upon heating that reversibly oxidizes upon cooling. The reduction process should be related to the release of oxygen with the concomitant vacancy formation within the structure due to the partial reduction of Fe^{4+} to Fe^{3+}. Similar trends were observed for the rest of the samples. However, the oxygen vacancy concentration produced upon heating increases with Ca content, as displayed in Figure 6b. Greater Ca content introduces a higher level of oxidized Fe^{4+} through charge compensation. This is then available for reduction at the high operating temperatures of IT-SOFCs, favoring the formation of oxygen vacancies. This is in agreement with the evolution of the crystal structure with Ca doping level discussed earlier. It is important to note that the introduction of oxygen vacancy defects is essential to induce mixed ionic-electronic conductivity in these materials, favoring the oxygen reduction behavior desirable for cathodic operation in IT-SOFCs.

In order to assess the suitability of the material's electrochemical behavior for application in SOFC cathodes, the polarisation resistance (R_p) was determined by impedance analysis of LCFN/SDC/LCFN symmetrical cells. Fabrication procedures have a

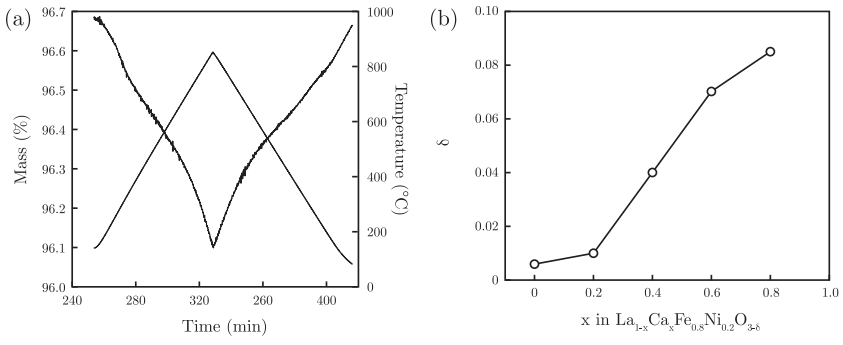

Figure 6. a) Thermogravimetric analysis in air of $La_{0.4}Ca_{0.6}Fe_{0.8}Ni_{0.2}O_{3-\delta}$ and b) evolution of the oxygen vacancy concentration (δ) with the Ca content at 900 °C.

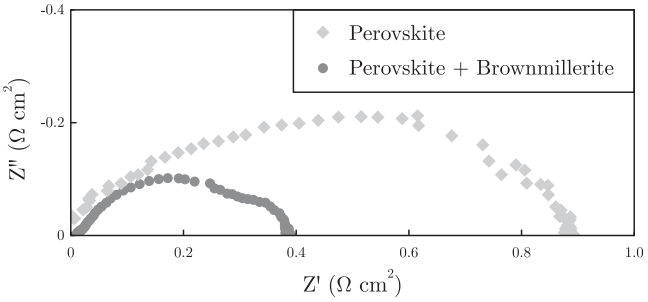

Figure 7. Impedance spectra of $La_{0.6}Ca_{0.4}Fe_{0.8}Ni_{0.2}O_{3-\delta}$ (perovskite) and $La_{0.3}Ca_{0.7}Fe_{0.8}Ni_{0.2}O_{3-\delta}$ (perovskite + brownmillerite).

huge effect on the performance and therefore on the electrochemical response of the materials. In previous work, studies were carried out in order to optimize the processing technique of the symmetrical cells, obtaining reproducible results for the $La_{0.6}Ca_{0.4}Fe_{0.8}Ni_{0.2}O_3$ cathode.[53,54] The results as a function of Ca content at 800 °C are shown in Figure 5. R_p can be seen to decrease with increasing Ca content up to 60–70%. Microstructure and R_p are strongly related and low density, small particle size materials have been seen to result in lower R_p values.[55,56] In this work, the sample microstructure was reported earlier to feature small particle sizes due to the liquid mix production method, and the porosity was seen to increase with Ca content up to the appearance of the brownmillerite phase at $x = 0.5$, which explains this initial drop in R_p. The samples with 60–70% Ca show the lowest resistance values which could be related to the higher oxygen vacancy content induced in these phases with increased Ca content, as evidenced by thermogravimetric analysis, and the presence of the brownmillerite phase. R_p is then seen to sharply increase for the samples with 80–90% Ca content. This increase could be related to the appearance of lanthanum oxide as an impurity, as corroborated by XRD analysis, and a loss of interconnected porosity associated with the agglomeration seen by SEM. In summary, these cathode materials present the best performance up to 50–70% Ca content.

Impedance spectra for the pure perovskite (LCFN0.4) and perovskite and brownmillerite (LCFN0.7) containing materials between 700–850 °C temperature range are presented in the Supporting Information, together with discussion of the featured processes. A direct comparison of these two materials is shown in **Figure 7**. As can be seen, at low frequency the semicircle is larger in the single phase material, providing a greater contribution to the total resistance of the electrode, while at high frequencies the semicircle differs very little between the two. This low frequency semicircle is considerably reduced when the brownmillerite phase appears, confirming that the diffusion of oxide ions generated in the material surface is facilitated by the appearance of the ionically conducting $Ca_2Fe_2O_5$-type phase. This behavior is similar to that observed for conventional composite cathodes.[57]

The dominant resistive process in these cathode materials is therefore the electrochemical resistance associated with oxygen exchange at the electrode surface. The corresponding semicircle in the impedance spectra is observed at low frequencies, indicating a large capacitance. This is a chemical capacitance related to oxygen stoichiometry changes in the electrode bulk. Thus, the dominating low frequency arc contains information on both the surface and the bulk of the electrode.

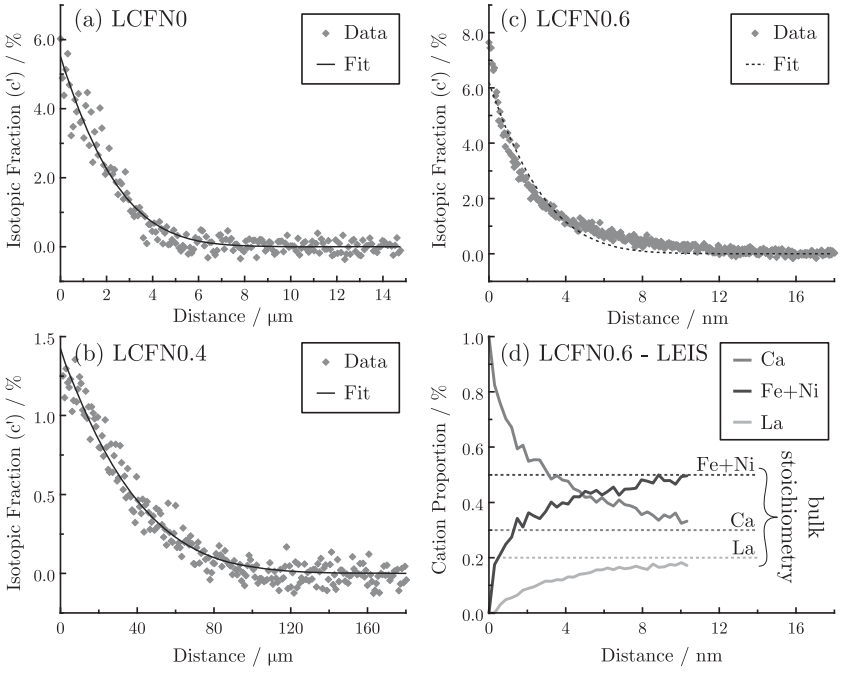

Figure 8. Oxygen-18 diffusion profiles in a) LCFN0, b) LCFN0.4 and c) LCFN0.6. All samples exchanged in an enriched ^{18}O gas at 800 °C in $pO_2 = 200$ mbar for t ≈10 min. Also shown is d) the surface depth-dependent composition in the LCFN0.6 determined by LEIS.

2.4. Oxygen Tracer Diffusion

In order to better understand the oxygen transport properties, tracer diffusion measurements were performed on three LCFN compositions, LCFN0, 0.4 and 0.6, by oxygen-18 isotope exchange and secondary ion mass spectrometry (SIMS). Oxygen tracer diffusion (D^*) and surface exchange (k^*) coefficients were obtained by non-linear least squares regression curve fitting of the measured diffusion profiles to the solution of Fick's second law solved for diffusion in a semi-infinite medium by Crank:[58]

$$C'(x,t) = \frac{C(x,t) - C_{bg}}{C_g(x) - C_{bg}} \quad (1)$$

where $C'(x, t)$ is the isotopic fraction of ^{18}O at depth x normalised to the annealing gas concentration, $C(x, t)$ is the experimentally determined isotopic fraction of ^{18}O at depth x, C_{bg} is the natural isotopic background level of ^{18}O, C_g is the isotopic fraction of ^{18}O in the enriched gas and t is time of anneal.

Figure 8 shows the three diffusion profiles. Considering first the LCFN0 (Figure 8a) and

LCFN0.4 (Figure 8b) compositions, both recorded utilizing a cross-sectional linescanning technique, it can be observed that the shape of the experimental profile matches the regression analysis based on Eq. (1) very well. The extracted oxygen tracer diffusion (D^*) and surface exchange (k^*) coefficients for the best performing single phase material, LCFN0.4 (779 °C, 200 mbar, 670 s), were measured as 2.2×10^{-8} cm^2 s^{-1} and 7.4×10^{-8} cm s^{-1}, respectively. The diffusivity value for LCFN0.4 is in good agreement with those reported in the literature for other state-of-the-art cathode perovskites and is, in fact, higher than that reported for LSM.[59] For comparison, Esquirol et al. studied the oxygen transport properties of $La_{0.6}Sr_{0.4}Co_{0.2}Fe_{0.8}O_3/Ce_{0.8}Gd_{0.2}O_2$ composites showing a D^* value of 4.18×10^{-8} cm^2 s^{-1} (exchanged 1800 s at 800 °C and 880 mbar).[60] In addition Steele et al. reported a D^* value of 2×10^{-8} cm^2 s^{-1} (T = 700 °C) for $La_{0.6}Ca_{0.4}Co_{0.2}Fe_{0.8}O_3$.[61] The ionic contribution to conductivity (σ_{ion}) can be calculated using the Nernst-Einstein relationship:[62]

$$\sigma_{ion} = \frac{z^2 e^2 c_{ion} D^*}{kT} \quad (2)$$

Where z is the valence of the ion, e is the charge on an electron, c_{ion} is the total concentration of the diffusing ion in the crystal, k is the Boltzmann constant and T is the temperature. For the LCFN0.4 material, measured at 779 °C and utilizing oxygen concentrations as determined by TGA at 900 °C, this equates to 1.9×10^{-3} S cm^{-1}. This is of the same order as some purely ionically conducting SOFC electrolytes such as $La_{9.5}Mn_{0.5}(GeO_4)_6O_{2.75}$ apatite (1×10^{-2} S cm^{-1} at 800 °C)[63] and close to that of widely used Y_2O_3-stabilised ZrO_2 (2.5×10^{-2} S cm^{-1} at 800 °C).[64]

The surface exchange ($k*$) value is, however, slightly lower than other cathode materials. $La_{0.6}Sr_{0.4}CoO_3$ is reported to have a $k*$ of 5×10^{-5} cm/s[65] while compositions with Fe B-site doping, such as $La_{0.6}Ca_{0.4}Co_{0.8}Fe_{0.2}O_3$ (2×10^{-5} cm/s[66]), $La_{0.6}Sr_{0.4}Co_{0.8}Fe_{0.2}O_3$ (5×10^{-5} cm/s[67]) and $La_{0.6}Sr_{0.4}Fe_{0.8}Co_{0.2}O_3$ (9×10^{-7} cm/s[68]), all feature $k*$ at 800 °C, 1 atm, between one and 3 orders of magnitude higher than in the LCFN0.4 material. This detrimental effect could be due to a Ca surface segregation effect, to be discussed shortly.

D^* and k^* for the LCFN0 sample (769 °C, 200 mbar, 800 s) are 6.4×10^{-11} cm^2/s and 1.4×10^{-8} cm/s, respectively. This displays a decrease in diffusivity compared to LCFN0.4 as expected from the significantly lower oxygen vacancy concentration determined by thermal analysis. The ionic contribution to conductivity determined by the Nernst-Einstein relationship (2) in this case is 5.7×10^{-6} S cm^{-1}. The surface exchange is, however, very similar for both compositions.

The high Ca content LCFN0.6 phase (Figure 8c) could only be collected utilising a sputter depth profiling technique due to a diffusion length significantly shorter than expected. The data also shows significant deviation from the regression analysis suggesting unsuitability of the simple model used. The fitting indicates a D^* and k^* of 8.8×10^{-17} cm^2 s^{-1} and 1.9×10^{-11} cm s^{-1}, respectively. The diffusion coefficient, in this case, is far lower than would be expected from the excellent electrochemical performance seen for this composition. The deviations from the fitting suggest that this is not merely diffusion through a homogeneous, single phase material. Low energy ion scattering (LEIS) was used in order to investigate the surface composition of the LCFN0.6 sample after isotope exchange. This revealed that the surface monolayer contained solely Ca and O, suggesting the presence of the binary oxide CaO. Utilising an additional sputtering beam, the depth dependence of the cation composition by LEIS is shown in Figure 8d. The CaO layer is seen to extend to just the first few nanometres. To the best of the authors' knowledge there have been no investigations of the self-diffusion of O anions in CaO. Considering the analogous MgO binary oxide, oxide ions in CaO can be estimated to have a D^* on the order of 10^{-19} cm^2 s^{-1}.[69] A continuous layer of CaO on the sample surface would therefore lead to a drastic reduction in the amount of isotope tracer reaching the bulk, resulting in levels too low as to be distinguished from background. The presence of Ca enrichment at the surface was also seen in LEIS analysis of the LCFN0.4 sample, albeit to a lesser extent, likely causing the apparent reduction in k^*. A full study of the surface segregation behavior of these materials, investigated by LEIS, will be presented in future work.

The presence of this CaO surface segregate is not seen to influence electrochemical measurements or appear in temperature dependent XRD analysis. This can be attributed to the difference in surface area of the samples. Those used in isotope exchange are highly dense, presenting a small surface area. The small volume percentage of CaO that segregates to the surface is capable of covering the entirety of the sample, in this case, and would not be within the detection limits of XRD. In the porous material of the symmetrical cell cathodes, the high level of porosity will increase the surface area per unit volume significantly, resulting in a non-continuous CaO layer. The value of diffusion coefficient (D^*) in the LCFN0.6 material is therefore non-representative of its in-situ behavior.

3. Conclusions

The $La_{1-x}Ca_xFe_{0.8}Ni_{0.2}O_{3-\delta}$ (LCFN, $0 \leq x \leq 0.9$) compositional range was investigated to determine suitability for application as cathode materials for IT-SOFCs, uncovering performance enhancing pseudo-composite materials at high Ca doping levels.

X-ray diffraction studies revealed single perovskite phase material in compositions with low levels of Ca A-site substitution ($x \leq 0.4$). The introduction of Ca enhances performance through the formation of oxygen vacancies, resulting in a steadily increasing conductivity and decreasing polarization resistance in symmetrical cells with Sm-doped ceria electrolytes. Measurement of the oxygen diffusion behavior reveals that 40% Ca substitution in $LaFe_{0.8}Ni_{0.2}O_{3-\delta}$ results in a 3 orders of magnitude enhancement of the oxygen ion conductivity. The presence of Ca is therefore fundamental for the introduction of oxygen vacancies and thus, ionic conduction. The highest performance, single-phase material is therefore $La_{0.6}Ca_{0.4}Fe_{0.8}Ni_{0.2}O_{3-\delta}$, which features high electronic and ionic conductivities of approximately 250 S cm^{-1} (600–800 °C) and 1.9×10^{-3} S cm^{-1} (800 °C), respectively.

Increasing the Ca content to 0.5 or greater results in the presence of a secondary phase, indexed to a brownmillerite-type

($Ca_2Fe_2O_5$) structure. This proves hugely advantageous, resulting in the pseudo-composite material exhibiting a significant performance improvement with the range, $0.5 \leq x \leq 0.7$, featuring the lowest R_p of 0.2 Ω cm^2. This is attributed to the ionic conductivity supplied by the brownmillerite phase. With Ca content greater than 0.7, performance degrades, ascribed to the simultaneous effect of additional segregated phases such as La_2O_3, and a coarsening of the microstructure leading to a decrease in the interconnected porosity required for oxygen reduction.

Summarizing the overall suitability of these materials for application as cathodes in IT-SOFCs, in the $0 \leq x \leq 0.7$ range, all materials feature conductivities over 100 S cm^{-1}, making them suitable for application, $x = 0.4$ is the highest performing single phase material with competitive levels of ionic conductivity, and pseudo-composite materials in the $0.5 \leq x \leq 0.6$ range feature extremely high electronic conductivities, the lowest polarization resistance and best thermomechanical compatibility with SDC.

4. Experimental Section

Sample Preparation: The liquid mix method was employed for the synthesis of $La_{1-x}Ca_xFe_{0.8}Ni_{0.2}O_{3-\delta}$ (LCFN) ($0 \leq x \leq 0.9$). Stoichiometric quantities of the nitrate salts [$La(NO_3)_3{\cdot}5H_2O$; $Ca(NO_3)_2{\cdot}H_2O$; $Fe(NO_3)_3{\cdot}9H_2O$; $Ni(NO_3)_2{\cdot}6H_2O$] and citric acid were dissolved in distilled water and a suitable volume of ethylene glycol was subsequently added. The resulting solution was agitated and heated on a hot plate until the formation of a gel. After that the gel, first treated in a sand bath, was calcined at 600 °C in an oven for 12 h with a 1 °C/min rate.

Characterization: The phase purity was verified by X-ray diffraction (XRD) using a Philips X'Pert-MPD (Bragg-Brentano geometry) diffractometer with CuKα radiation. The diffraction data was refined by the Rietveld method,[70] using Fullprof software.[71] The sample morphology was investigated with a JEOL JSM-6400 SEM, operating at an accelerating voltage of 20 kV. The thermal expansion coefficient (TEC) was measured with a LINSEIS vertical dilatometer (L75 Platinum Series). Dense sintered samples featuring parallel surfaces were thermally cycled in the temperature range of 200 to 1000 °C in air.

The electrical conductivity was measured in air using the Van der Pauw four probe technique. The oxygen vacancy content of each sample in the typical operational environment of a cathode in an SOFC (high temperature under air) was also evaluated and measured by thermogravimetry. For LCFN electrode characterization, $Sm_{0.8}Gd_{0.2}O_2$ electrolyte supported symmetric cells were fabricated. The symmetric cells were characterized by electrochemical impedance spectroscopy (EIS) in air from 850 ºC to room temperature using a Solartron 1260 Frequency Response Analyzer under open circuit voltage (OCV).

In order to investigate oxygen ion diffusion behavior, isotopic tracer self-diffusion measurements were performed on dense samples. A density of greater than 95% in all cases was sufficiently high to avoid fast gas diffusion through pores, artificially distorting the measured diffusion profiles[72]. Resulting profiles were measured by time-of-flight secondary ion mass spectrometry (ToF-SIMS) on a TOF.SIMS^5 instrument (ION-TOF GmbH, Münster, Germany). Surface compositional analysis was performed on the exchanged LCFN0.6 sample using low energy ion scattering (LEIS) on a Qtac 100 instrument (ION-TOF GmbH, Münster, Germany). Further details of all characterization methods are provided in the Supporting Information.

Supporting Information

Supporting Information is available from the Wiley Online Library or from the author.

Acknowledgements

This work has been partially financed by the Spanish CiCyT under project MAT2010-19442 and by the Government of the Basque Country under project IT- 312-07, IT 570-13 and SAIOTEK (S-PE11UN064 and S-PE12UN140). N.O.-V. thanks the University of the Basque Country (UPV/EHU) for funding her research activities under the "Especialización de Personal Investigador del Vicerrectorado de Investigación de la UPV/EHU" programme. This research was also supported by a Marie Curie Intra European Fellowship within the seventh European Community Framework Programme (PIEF-GA-2009-252711) (for M.B).

Received: February 5, 2013
Revised: March 26, 2013
Published online: April 30, 2013

[1] N. P. Brandon, S. Skinner, B. C. H. Steele, *Annu. Rev. Mater. Res.* **2003**, *33*, 183.
[2] L. Zhao, B. He, Y. Ling, Z. Xun, R. Peng, G. Meng, X. Liu, *J. Hydrogen Energy* **2010**, *35*, 3769.
[3] J. Chen, F. Liang, L. Liu, S. P. Jiang, L. Jian, *J. Hydrogen Energy* **2009**, *34*, 6845.
[4] L. W. Tai, M. M. Nasrallah, H. U. Anderson, D. M. Sparlin, S. R. Sehlin, *Solid State Ionics* **1995**, *76*, 273.
[5] H. Wang, C. Tablet, A. Feldhoff, J. Caro, *Adv. Mater.* **2005**, *17*, 1785.
[6] J. W. Stevenson, T. R. Armstrong, R. D. Carnein, L. D. Pederson, W. J. Weba, *J. Electrochem. Soc.* **1996**, *143*, 2722.
[7] P. Ciambelli, S. Cimino, L. Lisi, M. Faticanti, G. Minelli, I. Pettiti, P. Porta, *Appl. Catal. B* **2001**, *33*, 193.
[8] F. Tietz, A. Mai, D. Stöver, *Solid State Ionics* **2008**, *179*, 1509.
[9] E. Bucher, W. Sitte, F. Klauser, E. Bertel, *Solid State Ionics* **2011**, *191*, 61.
[10] R. Chiba, F. Yoshimura, Y. Sakurai, *Solid State Ionics* **1999**, *124*, 281.
[11] R. Chiba, F. Yoshimura, Y. Sakurai, *Solid State Ionics* **2002**, *152*, 575.
[12] H. Taguchi, Y. Masunaga, K. Hirota, O. Yamaguchi, *Mater Res. Bull.* **2005**, *40*, 773.
[13] M. B. Bellakki, V. Manivannan, P. McCurdy, S. Kohli, *J. Rare Earths* **2009**, *27*, 691.
[14] T. Montini, M. Bevilacqua, E. Fonda, M. F. Casulla, S. Lee, C. Tavagnacco, R. J. Gorte, P. Fornasiero. *Chem. Mater* **2009**, *21*, 1768.
[15] M. Mogensen, S. Primdahl, M. J. Jørgensen, C. Bagger, *J. Electroceram.* **2000**, *5*, 141.
[16] C. Sun, R. Hui, J. Roller, *J. Solid State Electrochem.* **2010**, *14*, 125.
[17] N. Ortiz-Vitoriano, I. R. de Larramendi, J. I. R. de Larramendi, M. I. Arriortua, T. Rojo, *J. Power Sources* **2011**, *196*, 4332.
[18] V. Dusastre, J. A. Kilner, *Solid State Ionics* **1999**, *126*, 163.
[19] K. Wang, R. Ran, W. Zhou, H. Gu, Z. Shao, J. Ahn, *J. Power Sources* **2008**, *179*, 60.
[20] J. Deseure, Y. Bultel, L. Dessemond, E. Siebert, P. Ozil, *J. Appl. Electrochem.* **2007**, *37*, 129.
[21] A. Jones, M. S. Islam, *J. Phys. Chem. C* **2008**, *112*, 4455.
[22] Y. H. Chen, Y. J. Wei, H. H. Zhong, J. F. Gao, X. Q. Liu, G. Y. Meng, *Ceram. Int.* **2007**, *33*, 1237.
[23] M. A. Ahmed, S. I. El-Dek, *Mater. Sci. Eng. B* **2006**, *128*, 30.
[24] R. D. Shannon, *Acta Crystallogr. A* **1976**, *32*, 751.
[25] K. Vidal, L. M. Rodríguez-Martínez, L. Ortega-San Martín, E. Díez-Linaza, M. L. Nó, T. Rojo, A. Laresgoiti, M. I. Arriortua, *Solid State Ionics* **2007**, *178*, 1310.
[26] M. A. Ahmed, R. Seoudi, S. I. El-dek, *J. Mol. Struct.* **2005**, *74*, 41.
[27] M. B. Bellakki, V. Manivannan, J. Das, *Mater. Res. Bull.* **2009**, *44*, 1522.
[28] J. Cihlar, D. Del Favero, J. Cihlar Jr., A. Buchal, J. V. Herle, *J. Eur. Ceram. Soc.* **2006**, *26*, 2999.

[29] L. A. Isupova, I. S. Yakovleva, S. V. Tsybulya, G. N. Kryukova, N. N. Boldyreva, A. A. Vlasov, G. M. Alikina, V. P. Ivanov, V. A. Sadykov, *Kinet. Catal.* **2000**, *41*, 287.
[30] A. M. Abakumov, M. G. Rozova, E. V. Antipov, *Rus. Chem. Rev.* **2004**, *73*, 847.
[31] A. Mitterdorfer, L. Glaucker, *Solid State Ionics* **1998**, *111*, 185.
[32] P. Berastegui, S. G. Eriksson, S. Hull, *Mater. Res. Bull.* **1999**, *34*, 303.
[33] C. Zuo, M. Liu, M. Liu, *Sol-Gel Processing for Conventional and Alternative Energy, Advances in Sol-Gel Derived Materials and Technologies* (Eds: M. Aparicio, A. Jitianu, L.C. Klein), Springer Science+Business Media, New York **2012**, Ch.2.
[34] N. Ortiz-Vitoriano, I. R. de Larramendi, I. G. de Muro, J. I. R. de Larramendi, T. Rojo, *Mater. Res. Bull.* **2010**, *45*, 1513.
[35] L. M. Hrovat, D. Kuscer, J. Holc, S. Bernik, D. Kolar, *J. Mater. Sci. Lett.* **1996**, *15*, 339.
[36] N. Sakai, T. Kawada, H. Yokokawa, M. Dokiya, I. Kojima, *J. Am. Ceram. Soc.* **1993**, *76*, 1551.
[37] V. V. Kharton, A. L. Shaulo, A. P. Viskup, M. Avdeev, A. A. Yaremchenko, M. V. Patrakeev, A. I. Kurbakov, E. N. Naumovich, F. M. B. Marques, *Solid State Ionics* **2002**, *150*, 229.
[38] A. Petric, P. Huang, F. Tietz, *Solid State Ionics* **2000**, *135*, 719.
[39] H. Ullman, N. Trofimenko, F. Tietz, D. Stöver, A. Ahmad-Khanlou, *Solid State Ionics* **2000**, *138*, 79.
[40] A. L. Shaula, Y. V. Pivak, J. C. Waerenborgh, P. Gaczyñski, A. A. Yaremchenko, V. V. Kharton, *Solid State Ionics* **2006**, *177*, 2923.
[41] K. Yao, X. Liu, P. Li, H. Liu, L. Gao, H. Wang, M. Zheng, W. Su, *Int. J. Hydrogen Energy* **2011**, *36*, 6123.
[42] K. J. Yoon, P. A. Zink, S. Gopalan, U. B. Pal, L. R. Pderson, *J. Electrochem. Soc.* **2009**, *156*, B795.
[43] F. Bridawn, S. Lee, J. M. Vohs, R. J. Gorte, *J. Electrochem. Soc.* **2008**, *155*, B660.
[44] M. Søgaard, P. V. Hendriksen, M. Mogensen, *J. Solid State Chem.* **2007**, *180*, 1489.
[45] J. Misuzaki, T. Sasamoto, W. R. Cannon, H. K. Bowen, *J. Am. Ceram. Soc.* **1983**, *66*, 247.
[46] E. Bucher, W. Sitte, *Solid State Ionics* **2004**, *173*, 23.
[47] H. Krüger, V. Kahlenberg, V. Petříček, F. Phillipp, W. Wertl, *J. Solid State Chem.* **2009**, *182*, 1515.
[48] J. B. Goodenough, J. E. Ruiz-Diaz, Y. S. Chen, *Solid State Ionics* **1990**, *44*, 21.
[49] Q. Li, L. Sun, L. Huo, H. Zhao, J. C. Grenier, *Int. J. Hydrogen Energy* **2010**, *35*, 9151.
[50] J. B. Goodenough, J. E. Ruiz-Diaz, Y. S. Chen, *Solid State Ionics* **1990**, *44*, 21.
[51] K. J. Yoon, P. A. Zink, S. Gopalan, U. B. Pal, L. R. Pederson, *J. Electrochem. Soc.* **2009**, *156*, B795.
[52] D. Kuscer, J. Holc, M. Hrovat, D. Kolar, *J. Eur. Ceram. Soc.* **2001**, *21*, 1817.
[53] N. Ortiz-Vitoriano, C. Bernuy-López, I. R. de Larramendi, R. Knibbe, K. Thydén, A. Hauch, P. Holtappels, T. Rojo, *Appl. Energy* **2013**, *104*, 984.
[54] N. Ortiz-Vitoriano, A. Hauch, I. R. de Larramendi, C. Bernuy-López, R. Knibbe, T. Rojo, *J. Power Sources* **2013**, DOI: 10.1016/j.jpowsour.2013.03.12.
[55] J. Schiemer, R. Withers, L. Norén, Y. Liu, L. Bourgeois, G. Stewart, *Chem. Mater.* **2009**, *21*, 4223.
[56] M. J. Jørgensen, S. Primhdal, C. Bagger, M. Mogensen, *Solid State Ionics* **2001**, *139*, 1.
[57] N. Ortiz-Vitoriano, I. R. de Larramendi, J. I. R. de Larramendi, M. I. Arriortua, T. Rojo, *J. Power Sources* **2011**, *196*, 4332.
[58] J. Crank, *Mathematics of Diffusion*, 2nd ed., Oxford University Press, London **1975**.
[59] S. Carter, A. Selcuk, R. J. Charter, J. Kajda, J. A. Kilner, *Solid State Ion.* **1992**, *53*, 597.
[60] A. Esquirol, J. Kilner, N. Brandon, *Solid State Ionics* **2004**, *175*, 63.
[61] B. C. H. Steele, *Solid State Ionics* **1996**, *86*, 1223.
[62] M. Barsoum, *Fundamentals of Ceramics*, Taylor and Francis, Abingdon **2003**.
[63] E. Kendrick, K. S. Knight, P. R. Slater, *Mat. Res. Bull.* **2009**, *44*, 1806.
[64] J. Herle, A. J. McEvoy, K. Thampi, *J. Mater. Sci.* **1994**, *29*, 3691.
[65] T. Kawada, K. Masuda, J. Suzuki, A. Kaimai, K. Kawamura, Y. Nigara, J. Misuzaki, H. Yugami, H. Arashi, N. Sakai, H. Yokokawa, *Solid State Ionics* **1999**, *121*, 271.
[66] S. Carter, A. Selcuk, R. J. Chater, J. Kajda, J. A. Kilner, B. C. H. Steele, *Solid State Ionics* **1992**, *53*, 597.
[67] R. J. Chater, S. Carter, J. A. Kilner, B. C. H. Steele, *J. Eur. Ceram. Soc.* **1993**, *12*, 79.
[68] S. B. Adler, J. A. Lane, B. C. H. Steele, *J. Electrochem. Soc.* **1996**, *143*, 3554.
[69] P. Kofstad, *Nonstoichiometry, Diffusion, and Electrical Conductivity in Binary Metal Oxides*, John Wiley and Sons, Inc. New York **1972**.
[70] H. M. Rietveld, *J. Appl. Crystallogr.* **1969**, *2*, 65.
[71] J. Rodríguez-Carvajal, *Phys. B* **1993**, *192*, 55.
[72] A. Esquirol, J. Kilner, N. Brandon, *Solid State Ionics* **2004**, *175*, 63.